Integration of Electrolyzer into Frequency Containment Reserve: Implications for Japan's Energy Transition

Hossam Ashraf*, Masahiro Mae*, Tsuyoshi Yoshioka*, Ryuji Matsuhashi*

Abstract

The growing integration of renewable energy in Japan's power grid is intensifying the need for fast and flexible frequency control resources. In this context, large-scale water electrolyzers (WEs) can offer green hydrogen production while providing ancillary frequency containment services. Accordingly, this study presents a dynamic and techno-economic assessment of a 1 GW alkaline WE participating in Japan's Frequency Containment Reserve (FCR) market. Specifically, a two-phase framework is established comprising a validation of the WE's transient response under official pre-qualification tests (PQTs) and Assessment II. Moreover, the second phase determines the optimal long-term operating schedule through a mixed-integer linear optimization based on real FCR capacity prices and Kyushu spot market data. Technically, the proposed controller achieves full PQTs compliance, in terms of 100% in-band tracking during normal operation and recovery to the rated 400 MW bid within 6.7 s during -1 Hz events, without overshoot or instability. Economically, FCR participation lowers the six-month net operating cost by approximately 9 billion JPY, reaching a best-week operational hydrogen cost of 63.77 JPY/Nm³ with no change in total hydrogen output. Finally, the controller's disk-margin analysis confirms wide robustness margins. These results demonstrate the dynamic and economic viability of gigawatt-class WEs in Japan's balancing market.

Key words : Alkaline electrolyzer; Frequency Containment Reserve; Dynamic validation; Techno-economic optimization

1. Introduction

The rapid expansion of renewable energy in Japan's power system has heightened stability issues. Thus, flexible resources become obligatory under such a decarbonized operation [1]. Conversely, conventional frequency containment reserve (FCR) has long relied on thermal generation. However, as renewable penetration increases, procuring FCR from demand-side and distributed energy resources (DERs) has become an urgent policy and engineering challenge. Accordingly, recent institutional developments are accelerating the integration of DERs into Japan's ancillary-service markets [2]. For instance, the Electric Power Reserve eXchange (EPRX) was launched in 2021, while FCR trading started in April 2024 [3].

Among emerging flexible loads, water electrolyzers (WEs) are significantly attractive due to their simultaneous contribution to green hydrogen production and grid stability through rapid power modulation [4]. Hence, several studies have demonstrated the feasibility of WEs for frequency regulation or reserve provision [5-7]. Nevertheless, in Japan, research on microgrid operation with WEs has evaluated their participation in the supplemental reserve (三次調整力②) market [8]. The results indicate measurable hydrogen cost reductions. However, they are limited to steady-state scheduling with idealized assumptions and sub-10 MW systems.

Furthermore, parallel studies on FCR aggregation using solid-oxide fuel cells and storage batteries have clarified technical requirements for distributed participation but focused on household-scale DERs [9]. However, no existing work has yet demonstrated a techno-economic framework that combines dynamic FCR compliance testing with large-scale WE scheduling under Japanese market rules. Moreover, thermal dynamics of megawatt-class electrolysis systems have not been incorporated into economic dispatch optimization, despite their relevance to sustained FCR delivery. Specifically, it directly influences auxiliary consumption, efficiency, and permissible ramp rates.

Consequently, to bridge the aforementioned gaps, this study develops and validates an integrated framework for a 1 GW alkaline WE participating in Japan's FCR market. Particularly, Section 2 presents an overview of the Japanese FCR framework, its technical requirements, pre-qualification procedures, and assessment criteria. Section 3 performs dynamic validation against official pre-qualification and Assessment II criteria using a MATLAB/Simulink model. Moreover, a mixed-integer linear optimization for long-term techno-economic scheduling using 2024 FCR and Kyushu spot prices is developed in Section 4. Finally, Section 5 summarizes the main outcomes of WE's participation in FCR market along with future work propositions.

Corresponding author; Hossam Ashraf,
E-mail : hossam@enesys.t.u-tokyo.ac.jp
*Department of Electrical Engineering and Information Systems, The University of Tokyo
7-3-1 Hongo, Bunkyo-ku, Tokyo 113-8656, Japan

Accordingly, through this combined approach, the paper offers:

1) the first dynamic-to-economic linkage of a gigawatt-scale WE under Japan's FCR requirements,
2) quantitative insight into cost reductions and penalty avoidance enabled by FCR participation, and
3) evidence that incorporating thermal behavior improves dispatch realism and hydrogen-cost accuracy.

The findings provide practical guidance for Japan's ongoing effort to mobilize large-scale electrolysis as a flexible asset to support both power-system stability and hydrogen-supply cost reduction.

2. FCR Market Overview

Principally, Japan's FCR market is the fastest balancing service procured by the organization for cross-regional coordination of transmission operators (OCCTO) through the EPRX platform [3]. Introduced in 2024, it enables both generation- and demand-side assets to autonomously provide symmetric primary frequency regulation for 50/60 Hz systems. Each FCR product covers a 3-hour block traded weekly, while the minimum bid is 1 MW with 1 kW steps [1,2].

Technically, the FCR service requires participating facilities to autonomously adjust active power output or consumption according to instantaneous frequency deviations. A symmetric bid must provide both upward and downward regulation continuously within a narrow dead zone of ± 0.01/0.012 Hz around the nominal frequency 50/60 Hz, respectively. Additionally, the relationship between frequency deviation and active power change follows a proportional droop characteristic, limited to 5%.

2.1 Pre-qualification tests

Before admission, every resource undergoes a pre-qualification test (PQT) sequence defined by OCCTO. It consists of normal and abnormal evaluation periods. During the normal test, a 30-min sequence of small frequency deviations, for example between ±0.01 Hz and ±0.16 Hz for 60 Hz, is applied. The output power change must remain within ±10% of the theoretical droop-based target for at least 90% of 1-s sampled data points. This ensures a stable proportional response without overshoot or oscillation under minor frequency variations [10].

On the other side, the abnormal test occurs when the system frequency deviation exceeds ±1.0 Hz. Hence, the resource must start its power response within 2 s, reach the full theoretical droop-based output within 10 s, and sustain at least 90% of that level for ≥ 300 s. These limits confirm the provider's capability to deliver continuous and reliable control under severe frequency depression or rise.

2.2 Operational assessments

After qualification, two performance assessments govern market participation. Specifically, Assessment I is conducted before each delivery period to verify that the offered reserve capacity per 3-h block is physically feasible. Any shortfall between the contracted and deliverable amount incurs a penalty, as described in (1) [10].

$$Penalty\ I = 1500 \times p_{FCR}(b) \times S(b) \qquad (1)$$

where, $p_{FCR}(b)$ [JPY/kW/30 min] is capacity price for block b and the reserve shortfall is expressed by $S(b)$ [MW].

Furthermore, Assessment II re-examines real-time frequency-response quality using operational data. During normal operation, the evaluation focuses solely on response direction, whether the actual power change follows the same sign as the theoretical droop command during frequency deviations. Conversely, when abnormal frequency deviations are greater than or equal to 0.2 Hz, the unit must start responding within 2 s, reach the full droop-based output within 10 s, and sustain ≥ 90% of that level for ≥ 300 s. Graphically, the droop characteristic defining the operational behavior of the participating resource is illustrated in **Fig. 1**.

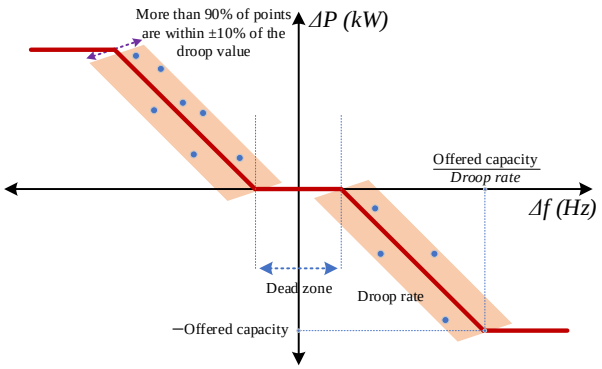

Fig.1 Frequency-power droop characteristic of FCR resources

It should be noted that the same curve applies to both generating and consuming resources. However, for demand-side resources (e.g. WEs), the direction of active-power change is inverted, where a reduction in demand corresponds to a positive reserve contribution. It's worth mentioning that failing in Assessment II results in forfeiture of the awarded capacity fee for the affected 3-h block. In other words, the provider does not receive capacity payment for that tranche.

3. Dynamic Validation of FCR Compliance

Unlike previous studies that only analyzed static or market-based participation, this work develops a physics-based dynamic model integrated with a compliance evaluation layer. This layer mirrors the official OCCTO pre-qualification and assessment criteria. Practically, this phase aims to demonstrate how a proper

control tuning of an WE can achieve the fast, accurate, and sustained response mandated for ancillary-service accreditation.

3.1 Model configuration and control structure

A transfer function-based model is derived here for a practical 1 GW WE plant, as described in (2) [11,12]. Physically, the plant minimum (P_{min}), maximum (P_{max}), and initial (P_{int}) operating powers are 200 MW, 1000 MW, and 600 MW, respectively.

$$\frac{\Delta P_{we}}{\Delta P_{ref}} = e^{-0.019s}\frac{1.0184}{(1+1.4809s)} \quad (2)$$

where, ΔP_{ref} [MW] and ΔP_{we} [MW] are the theoretically commanded and actual change in WE power.

The control architecture consists of a droop-based frequency-power conversion block, a feedback controller, and the physical plant, as shown in **Fig. 3**. The frequency deviation (Δf) [Hz] is first translated into the theoretical power reference (ΔP_{ref}) according to the droop gain (K_{droop}) [MW/Hz], given by (3).

$$K_{droop} = \frac{P_{rated}}{R \times f_{rated}} \quad (3)$$

where, P_{rated} [MW] is the WE's rated power, R [%] represents the droop rate, and f_{rated} [Hz] is the system rated frequency. Numerically, for $P_{rated} = 1000\ MW$, $R = 5\%$, and $f_{rated} = 50\ Hz$, $K_{droop} = 400\ MW/Hz$.

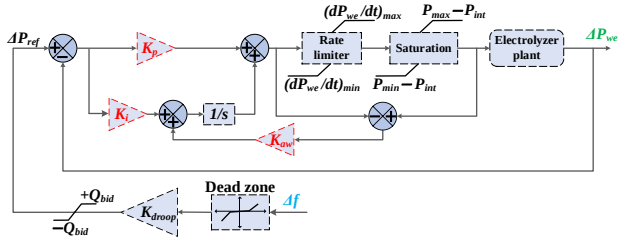

Fig. 2 Control architecture of the WE's FCR response

A dead zone of ±0.01 Hz suppresses unnecessary activation during normal operation, while the saturation ensures that the demanded reserve does not exceed the contracted FCR capacity (Q_{bid}) [MW]. It's worth highlighting that the maximum allowable symmetric Q_{bid} is 400 MW according to the WE's physical constraints. The resulting reference signal is tracked by a proportional–integral (PI) controller with anti-windup compensation.

Fundamentally, the PI controller is chosen for its ability to achieve zero steady-state error under step disturbances while maintaining a low-order, robust implementation suitable for large industrial power converters. The anti-windup mechanism mitigates integrator saturation when the actuator is constrained. Thereby the recovery speed is enhanced and the control bias after prolonged frequency events is avoided. Downstream of the PI stage, a rate limiter is included to emulate the physical slew constraints of the power electronics and hydrogen-pressure regulation system. Mainly, it prevents unrealistically fast current changes that could endanger stack integrity. The saturation block further bounds the actual stack power within P_{min} and P_{max}, enforcing operational safety and compliance with manufacturer limits.

3.2 Optimization framework

To ensure compliance with the FCR dynamic performance criteria, the controller parameters were tuned through an optimization procedure that embeds all PQTs' metrics directly within the objective function (OF). Accordingly, the decision vector (x) comprises the proportional (K_p) and integral (K_i) gains, and the anti-windup factor (K_{aw}). Each candidate vector is simulated over a 3600 s sequence consisting of the normal-period and abnormal-period test signals. From these simulations, a scalar performance index $J(x)$ is computed as the weighted sum of eight non-negative penalties reflecting the official OCCTO evaluation logic, as described in (4).

$$J(x) = 80(J_{stay} + J_{start} + J_{reach} + J_{sus}) + 10(J_{rtn} + J_{ovs}) + 2(J_{sm} + J_{sat}) \quad (4)$$

where, J_{stay} penalizes insufficient in-band duration (target ≥ 90%) during the normal period. J_{start}, J_{reach}, and J_{sus} correspond respectively to the FCR abnormal-period requirements that WE must start its power response within 2 s, reach the full theoretical droop-based command within 10 s, and sustain at least 90% of the bid power for ≥ 300 s. Additionally, smaller weights address secondary behaviors including J_{rtn} for return-to-baseline accuracy, J_{ovs} for overshoot magnitude, J_{sm} for power-ramp smoothness, and J_{sat} for actuator dwell at saturation. Hence, the OF is formulated as in (5).

$$OF = \min\left(J(x)\right) \quad (5)$$

It's obvious that the search space is highly nonlinear and discontinuous since the time-domain events introduce non-smooth performance surfaces. For this reason, the well-known particle swarm optimizer (PSO) is adopted due to its ability to handle discontinuous objective landscapes and its proven efficiency in controller tuning for nonlinear dynamic systems [13,14]. Basically, it avoids entrapment in local minima that frequently occurs when performance metrics involve time delays, saturation limits, and rate constraints. Furthermore, the resulting optimal parameters are subsequently validated using a disk-margin robustness analysis that confirms adequate gain- and phase-margin stability of the closed-loop WE control under modeling and parameter uncertainties.

3.3 Event generation and test protocol

To evaluate FCR compliance, the dynamic response of the WE control loop is tested using real and synthetic frequency trajectories that replicate the OCCTO's PQTs and Assessment II

requirements. A complete 3600 s simulation sequence is implemented combining normal and abnormal periods.

The normal-period integrates the first 30-min block combining realistic 50 Hz fluctuations measured on July 24th, 2025, from 5:00 to 5:30 PM at Matsuhashi lab, The University of Tokyo.

On the other side, the abnormal-period test introduces step-like under-frequency events of magnitude -1.0 Hz, each representing an FCR activation request. Four abnormal events are inserted in the second 30-min abnormal block, separated by sufficiently long gaps to observe return-to-baseline behavior. Each event follows a trapezoidal frequency pattern: a ramp down to -1 Hz, a 300 s hold, and a ramp back to 0 Hz. The resulting theoretical droop response serves as the reference trajectory against which start, rise, sustain, overshoot, and recovery metrics are evaluated.

All dynamic signals are simulated at 0.1 s resolution to capture sub-second transients. However, scoring follows the OCCTO time bases of 1 s for normal evaluation and 0.1 s for abnormal assessment. Therefore, each optimization iteration represents a full PQTs' cycle.

3.4 Optimization results

The PSO-optimized controller parameters are summarized in **Table 1** after 10 independent runs. Each execution includes 100 iterations and 25 populations.

Table 1 Optimal controller parameters

Parameter	K_p	K_i	K_{aw}	$J(x)$
Value	2.1585	2.1044	6.3959	0.6887

These values represent the best trade-off between fast activation, stable tracking, and minimal saturation while satisfying all FCR's PQTs' requirements. It's worth mentioning that Q_{bid} was fixed at 400 MW, representing the maximum headroom permitted between the rated and initial operating points. Similarly, the ramp-rate limits were fixed based on industrial data for large alkaline WE, 5 %/s for ramp-up and 20 %/s for ramp-down of rated power.

3.4.1 Pre-qualification results

During the normal-period operation of the PQT, the system maintained an in-band stay ratio of 100%, surpassing the ≥ 90% threshold. The measured frequency and corresponding power traces are shown in **Fig. 3(a)-(b)**, respectively, confirming that the WE power closely followed the reference within ±10% of the droop target throughout the 30-min window.

Furthermore, the abnormal-period response exhibits similarly precise behavior across four consecutive -1.04 Hz events, as revealed in **Fig. 4**. The WE initiated its response within 0.10 s, reached the full 400 MW target within 6.7 s, and sustained at least 90% of Q_{bid} for 306 s per event.

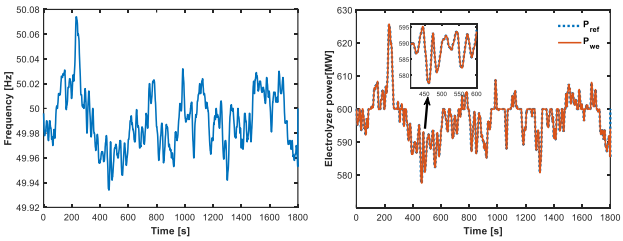

(a) Frequency measures (b) WE's power trajectory

Fig. 3 Normal-period response for PQT

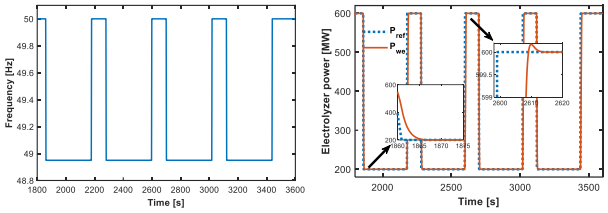

(a) Frequency measures (b) WE's power trajectory

Fig. 4 Abnormal-period response for PQT

In addition, the maximum overshoot observed during return-to-baseline was 0.03%, indicating excellent damping and control smoothness.

3.4.2 Assessment II results

The Assessment II validation further examined the controller's behavior under mixed-frequency conditions combining mild deviations, dead zone intervals, and two abnormal events. As depicted in **Fig. 5**, the system exhibited consistent bidirectional droop control.

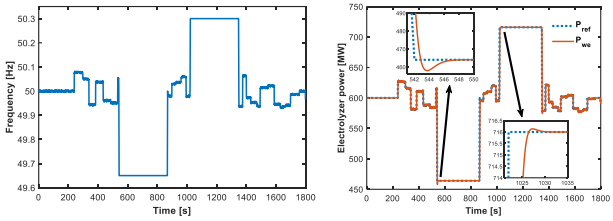

(a) Frequency measures (b) WE's power trajectory

Fig. 5 Assessment II response

According to **Fig. 5(b)**, the in-band stay ratio during normal operation was 99.7%. For the under-frequency event (−0.35 Hz), the power increased immediately (0.1 s start delay), reached the theoretical droop level within 1 s, and showed only 1.3% overshoot. During the over-frequency event (+0.30 Hz), the corresponding decrease reached its target within 4.5 s with a negligible 0.02% overshoot. Consequently, all dynamic metrics remained well within the prescribed 2 s / 10 s / 300 s limits.

Finally, the combined PQTs and Assessment II outcomes demonstrate that the optimized PI controller ensures high-fidelity tracking and robust dynamic performance for a GW-class alkaline WE. These experimentally validated parameters and limits form the technical foundation for the upcoming techno-economic

scheduling optimization, where market participation and hydrogen-cost reduction potential are quantitatively analyzed.

3.5 Controller Robustness and Disk-Margin Validation

To validate the robustness of the optimized PI + anti-windup controller beyond time domain performance, a frequency domain disk-margin analysis [20] was performed on the linearized WE loop. In this context, **Fig. 6(a)** illustrates the Nyquist-based disk margin envelope for simultaneous gain and phase perturbations. The system exhibits a disk margin radius of 1.66, corresponding to a simultaneous gain margin between 0.092 and 10.84 (±20.7 dB) and a phase margin of ±79.5° at the worst-case frequency of 1.32 rad/s. These wide stability margins indicate strong tolerance to parametric uncertainties and actuator nonlinearities inherent to large-scale alkaline systems.

Moreover, the closed-loop sensitivity peaks are modest (M_s=1.03 at 23.5 rad/s and M_t=1.01 at 0.46 rad/s), confirming well-damped disturbance rejection and minimal resonance amplification. Furthermore, as shown in **Fig. 6(b)**, the closed-loop step response of the linearized model demonstrates rapid settling without overshoot, verifying effective dynamic regulation under frequency deviations.

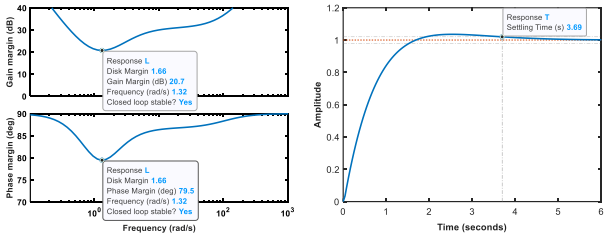

(a) Disk-margin analysis (b) Closed-loop step response

Fig. 6 Robustness and dynamic response of WE control loop

4. Scheduling Optimization under FCR Participation

Building upon the validated dynamic performance earlier achieved, this section develops a techno-economic scheduling framework to evaluate the profitability and operational feasibility of the 1 GW alkaline WE in Japan's FCR market.

4.1 Optimization model formulation

Basically, the proposed framework jointly optimizes the plant's electrical, hydrogen, and thermal domains over a rolling planning horizon, as illustrated schematically in **Fig. 7**.

In this configuration, the WE is connected to the AC grid through an AC/DC converter, which governs the power exchange and enables frequency-responsive operation. The DC side feeds the WE stack, the thermal-management unit, and the other balance-of-plant (BoP) auxiliaries.

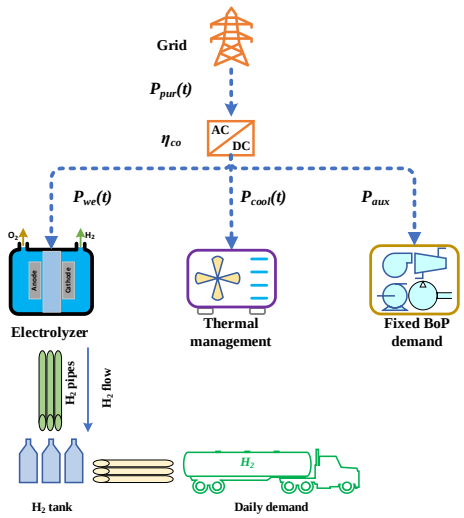

Fig. 7 Schematic of the techno-economic scheduling model

Hydrogen generated by the stack is stored in a high-pressure tank and subsequently delivered to end-use demand. Consequently, this integrated representation allows the optimization framework to simultaneously consider power balance, hydrogen storage dynamics, and thermal constraints within the FCR market structure.

Thus, this scheduling problem is formulated as a mixed-integer linear programming (MILP) model solved in MATLAB [17]. For each 30-min interval, the optimizer determines the WE power set-point P_{we} [MW], on/off state U_{we}[0/1], reserve capacity Q_{bid} [MW], hydrogen delivery D_{dlv} [Nm^3], and cooling power P_{cool}[MW], while satisfying market and physical constraints. A receding-horizon approach (7-day window, 1-day commitment) is used to ensure temporal consistency in tank level and temperature while maintaining computational tractability.

At each 30-min interval, the optimizer determines the operating state vector, as formulated in (6), to minimizes the total operational cost (C_{tot}) [JPY] over the scheduling horizon, as described by (7).

$$x(t) = \{P_{elr}, U_{elr}, Q_{bid}, S_b, D_{dlv}\} \quad (6)$$

$$C_{tot} = \sum_t \left[C_{pur}(t)P_{pur}(t)\Delta t - Q_{bid}(t)p_{FCR}(b) + Penalty\ I\right] \quad (7)$$

where, C_{pur} [JPY/kWh] denotes the all-in electricity purchase price (spot + surcharges), P_{pur} [MW] is the imported grid power, and p_{FCR} [JPY/kW/30 min] is the FCR capacity price per 3-h block (b).

Principally, the proposed model is subjected to a set of physical limits, thermal constraints, and market rules. First, the power balance that governs each 30-min slot is given by (8).

$$P_{pur}(t) = \frac{P_{we}(t)+P_{col}(t)+P_{aux}}{\eta_{co}} \quad (8)$$

where, P_{aux} [MW] represents a fixed BoP demand and $\eta_{co} = 0.98$ is the converter efficiency.

Additionally, the WE operating point and ramp limits are bounded by (9)-(10), respectively.

$$P_{min}U_{we}(t) \le P_{we}(t) \le P_{max}U_{we}(t) \quad (9)$$

$$|Q_{bid}(b) - P_{we}(b-1)| \le R_R \quad (10)$$

where, R_P [MW/slot] denote the WE's ramp limits between consecutive 30-min slots, respectively.

On the other side, reserve and shortfall constraints follow the OCCTO market design, as expressed in (11).

$$S(b) \ge Q_{bid}(b) - \frac{P_{we}(t)-P_{min}}{\eta_{co}} \quad (11)$$

Furthermore, the hydrogen-tank dynamics are represented by (12).

$$H_{tank}(t+1) = H_{tank}(t) + \phi_{H_2}P_{we}(t)\Delta t - D_{dlv}(t) \quad (12)$$

$$0 \le H_{tank}(t) \le H_{max}$$

where, H_{tank} [Nm^3] is the hydrogen content in the tank, ϕ_H [Nm^3/MWh] is the hydrogen production rate, and H_{max} [Nm^3] represents the maximum storage limit of the tank. D_{dlv} [Nm^3/30-min] refers to the hydrogen delivered to demand per slot, which is limited to a maximum value D_{max} [Nm^3] and tied to the total demand hydrogen per day D_{day} [Nm^3], as described by (13).

$$\sum_{t\in d} D_{dlv}(t) \ge D_{day}, \quad 0 < D_{dlv}(t) \le D_{max} \quad (13)$$

Finally, the first-order thermal model, presented in [4], is simply discretized, as formulated in (14). This discrete thermal model adopts a time constant of approximately 1.4 h, capturing the stack's inherent thermal inertia.

$$T_{we}(t+1) = a_{\mathrm{th}}T_{we}(t) + b_{heat}P_{we}(t) - d_{cool}P_{cool}(t) \quad (14)$$

where, the WE's temperature is symbolized by T_{elr} [°C]. a_{th} is the thermal inertial coefficient, b_{heat} [°C/MW] is the heating coefficient due to stack power, and d_{cool} [°C/MW] is the cooling coefficient due to BoP power.

In fact, several studies have indicated that alkaline WEs typically operate within a temperature range of 60-90 °C [6,15,16]. Thus, this model enforces these thermal limits while maintaining a comfort range of 70-80 °C regulated through $P_{cool} \in [0,100]$ MW. Deviations from the comfort band are linearly penalized in the objective function to ensure thermal safety without incurring unnecessary BoP energy consumption.

4.2 Data sources and parameter settings

The MILP scheduling framework employs real market data and experimentally grounded plant parameters to represent the techno-economic behavior of a 1 GW alkaline WE operating within the Japanese FCR market. Specifically, two main datasets are incorporated: (i) six monthly FCR capacity-price datasets from July to December 2024 [18], and (ii) the JEPX spot-price dataset for the same period, both featuring 30-min resolution [19]. Each FCR dataset provides the average clearing price and time stamps that align with the corresponding JEPX entries.

Kyushu is selected as the reference area because it exhibits Japan's highest solar-power penetration and frequent photovoltaic curtailment. Thus, more hours of very low or even negative prices are screened. This makes Kyushu an analytically valuable case for low-cost electrolysis.

Hence, the total electricity purchase cost per slot C_{pur} is calculated as the sum of the JEPX Kyushu spot price and region-specific surcharges. Particularly, the surcharges include a wheeling rate of 1.27 JPY/kWh, a renewable-energy surcharge 3.98 JPY/kWh, and a non-fossil certificate fee 0.40 JPY/kWh.

The physical and operational parameters are derived from practical alkaline WE specifications and the validated dynamic model in Section 3. The hydrogen storage and delivery parameters are scaled from aggregated 1-10 MW alkaline units[8], while all remaining constants and market settings are summarized in **Table 2**.

Table 2 Main parameters and constraints used in the MILP

Parameter	Parameter	Value
P_{aux}	Fixed auxiliary load.	140 MW
R_P	Set-point ramp limit (30-min).	±100 MW/slot
ϕ_{H_2}	H_2 yield per MWh.	200 Nm³/MWh
H_{max}	Tank capacity.	0.54 MNm³
D_{max}	Max delivery rate.	0.2 MNm³/30 min
D_{day}	Minimum daily delivery requirement.	2.88 MNm³/day
Gap tolerance	MILP optimality gap.	3%
Time limit	Max solve time per window.	300 s
Window length	Rolling horizon span.	7 days
Commitment step	Decision lock-in interval.	1 day

4.3 Optimization results

Before presenting the numerical results, the key assumptions of the optimization are summarized. Since the WE is assumed to have passed Assessment II, modeling its activation behavior would require embedding high-frequency dynamics into the MILP, making the problem computationally unsolvable. Thus, this phase considers only capacity provision, not real-time activation energy.

Table 3 Whole-period economic outcomes (July-December 2024)

Scenario	Energy Cost [MJPY]	FCR Revenue [MJPY]	Assessment-I Penalty [MJPY]	Net Cost [MJPY]	H_2 Delivered [MNm³]	Net H_2 Cost [JPY/Nm³]
With FCR	56471.842	10588.149	0.503	45884.196	529.92	86.59
No FCR	54869.802	×	×	54869.802	529.92	103.54

To ensure temporal consistency and comparability among results, only full seven-day market weeks (Saturday 00:00-Friday 23:30) are retained for key performance indicator (KPI) evaluation and plotting. Moreover, the optimization is performed in a deterministic framework. No price forecasting or stochastic modeling is applied. Instead, actual historical market prices are used directly as perfect-foresight inputs. This approach isolates the structural performance of WE-market interaction without the confounding effects of forecast error.

Furthermore, surplus hydrogen production is permitted, and there is no upper cap on daily delivery. This allows the optimizer to exploit low-price periods or high FCR revenues to produce additional hydrogen. Finally, the hydrogen tank acts as a temporal buffer, enabling energy-to-hydrogen time-shifting between high- and low-price periods while ensuring that daily contractual demand is always satisfied. Such assumptions provide a neutral baseline for assessing the intrinsic economic impact of FCR participation under real market conditions.

4.3.1 Whole-period performance

Herein, the aggregated techno-economic outcomes for July-December 2024 under the with FCR and no FCR scenarios are captured in **Table 3**. It's clear that participation in the FCR market substantially enhances the WE's profitability. Numerically, the total net operating cost decreases by approximately 9 billion JPY, accompanied by no change in hydrogen production. Consequently, the unit hydrogen cost declines from 103.54 JPY N/m³ to 86.59 JPY N/m³, a 16% improvement in cost efficiency.

4.3.2 Daily operational dynamics

Daily variations in cost and revenue illustrate how market conditions shape WE's operating schedule. In **Fig. 8(a)**, each day's bar shows the absolute magnitudes of cost, revenue, penalty, and the resulting net value plotted as separate stacked components. This allows direct comparison of each component's daily contribution, rather than viewing the bars as parts of the net cost.

On average, each day incurred 306.9 MJPY in electricity cost, earned 57.5 MJPY in reserve revenue, and paid almost zero MJPY in penalties, resulting in a mean net cost of ≈ 249.4 MJPY/day.

The dispersion of daily net cost (10-90% range = 197.7-315 MJPY day⁻¹, σ ≈ 46 MJPY) underscores the strong price sensitivity of the FCR-coupled operation. Notably, the lowest-cost day occurred on 13 October 2024 (151.5 MJPY), while 30 August 2024 marked the most expensive (458.7 MJPY). Seasonally, higher summer spot prices led to temporary net-cost peaks in August, whereas November exhibited the most favorable economics.

4.3.3 Hydrogen-storage behavior

The hydrogen-tank trajectory highlights the system's effective buffering capability under favorable market conditions, as revealed in **Fig. 8(b)**. In the best-performing week, the tank exhibits a substantial net increase, rising from 13,600 Nm³ at the start to 251,171 Nm³ at the end, an accumulation of ≈238,000 Nm³ (44% of capacity). Moreover, the SOC remained within 0-66% of the 0.54 MNm³ storage capacity, with no hard-limit violations, confirming adequate headroom for multi-day flexibility. Furthermore, hydrogen deliveries reached 20.16 million Nm³, exactly meeting the weekly contractual requirement (100%). On the other hand, the low-inventory periods (<15% SOC) accounted for only 34.5 hours. Additionally, daily fluctuations were well managed, with the largest single-day withdrawal reaching 78,029 Nm³ and the largest refill 237,200 Nm³. Overall, these results show that the storage system successfully smooths intra-week variability in production and demand.

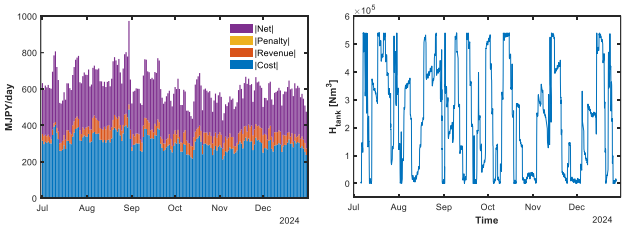

(a) Daily economics trends (b) Hydrogen-tank inventory

Fig. 8 Daily economic and hydrogen storage dynamics

4.3.4 Thermal and BoP performance

Thermal stability remained well within design boundaries, proving the integrated cooling strategy's superiority to maintain safe operation. According to Fig. **9(a)**, the mean stack temperature was ≈ 75 °C, with an absolute range of 60-86.7 °C and no events exceeding 90 °C. Approximately 93.9% of operation occurred

within the 70-80 °C comfort zone, while only 145.5 h fall below 70 °C and 124.0 h exceed 80 °C.

On the other hand, the BoP cooling operated during 6.2% of the time at an average 1.38 MW (max ≈ 80 MW). Statistically, this corresponds to 6.1 GWh or roughly 0.2% of total imported energy, as seen in **Fig. 9(b)**. The control slope averaged 8 MW °C⁻¹, and about 255 sizable intervention bursts (> 20 MW) were triggered for transient temperature corrections.

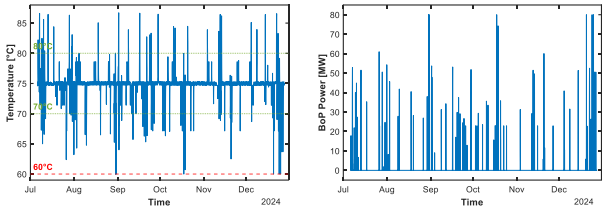

(a) Stack-temperature profile (b) BoP cooling activity

Fig. 9 WE's thermal response

4.3.5 Assessment I compliance

Reserve sufficiency across all 8832 slots validates the WE's physical readiness for FCR dispatch. Only 1.2% of slots exhibited shortfalls, primarily when the stack operated near its maximum limit, as illustrated in **Fig. 10(a)**. Average and peak shortfalls were 1 MW and 1 MW, respectively, resulting in a total Assessment-I penalty of ≈ 0.5 MJPY. The mean offered reserve capacity was 362.3 MW, with the bid saturating at its upper bound (95% of bids = 400 MW).

4.3.6 Ramp-rate flexibility

The optimized schedule leverages the WE's intrinsic flexibility for rapid power adjustments. Half-hourly power ramps averaged 12.6 MW, with 95% events below 100 MW and absolute maxima approaching 1000 MW, as elucidated in **Fig. 10(b)**. Approximately, 7.8% of ramps exceeded 75 MW, whereas 90.6% remained below 25 MW. Such results indicate that most transitions were modest while occasional larger steps ensured effective grid-balancing capability.

It's important to mention that the occasional ramp magnitudes above the nominal 100 MW/slot limit don't represent constraint violations but arise during start-up/shut-down transitions or between rolling-horizon windows. This is an intentional relaxation to maintain feasibility and continuity of operation.

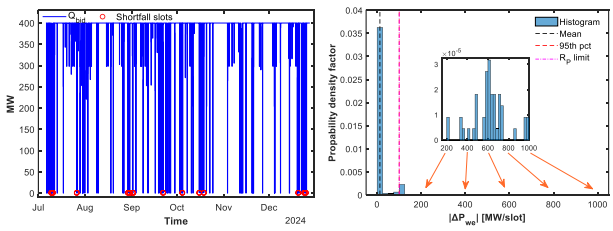

(a) Offered vs. actual reserve (b) Power-ramp magnitudes

Fig. 10 Assessment I compliance and ramp-rate flexibility

Now, needless to say that the six-month techno-economic simulation demonstrates that FCR participation substantially enhances the profitability and utilization of a 1 GW alkaline WE without violating thermal or operational constraints.

4.4 Market Week Variability

Herein, the weekly net cost and hydrogen cost evolution across the six-month horizon are recorded in **Fig. 11**. During the best market week (2-8 November 2024), the WE operated near optimal utilization, achieving a net cost of 1285.5 MJPY and a hydrogen cost of only 63.77 JPY/Nm³. The system sustained an average stack load of 607.05 MW with 385.1 MW of reserve capacity. This enables high participation in both energy and reserve markets. Moreover, the hydrogen tank operated between 0 and 66% of its capacity, indicating active buffering to capture low-price periods. Additionally, the thermal management system remained efficient, with 97.02% of the week within the 70-80 °C comfort zone and BoP power consumption limited to ≈ 0.05 % of imported energy.

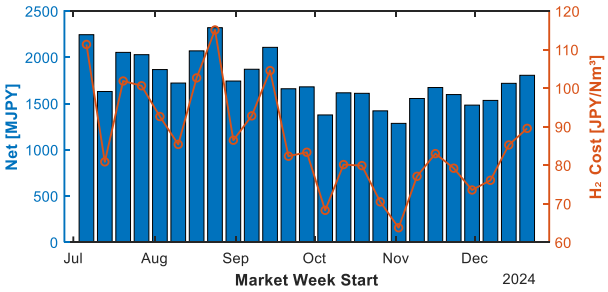

Fig. 11 Weekly net and hydrogen cost distribution

In contrast, the worst week (24-30 August 2024) coincided with depressed FCR prices and elevated spot-market costs. Hence, a net cost of 2320.18 MJPY and an increased hydrogen cost of 115.09 JPY/Nm³ are achieved. Furthermore, both average load (589.6 MW) and reserve provision (344.42 MW) declined, while the tank remained fully utilized. In addition, the thermal performance also deteriorated, with comfort compliance reduced to 91.37% of the week and BoP energy share rising to 0.38% due to frequent cooling demand at suboptimal operating points.

Lastly, **Table 4** consolidates key weekly performance indicators for the five best and five worst weeks, along with the median case.

5. Conclusion and Future Work

This study established a comprehensive framework for assessing the technical and economic viability of a 1 GW alkaline WE participating in Japan's FCR market. The proposed methodology effectively integrates dynamic validation and long-term market scheduling under real operational constraints.

Table 4 Weekly KPI Summary

Class	Week start	Net [MJPY]	H_2 cost [JPY/Nm^3]	Avg. Q_{bid} [MW]	Avg. P_{we} [MW]	Comfort T_{we} zone [%]	BoP share [%]	Tank util. [%]
Best	**02-Nov-24**	**1285.5**	**63.77**	**385.1**	**607.05**	**97.02**	**0.05**	**66**
Best	05-Oct-24	1376.65	68.29	368.21	615.6	93.75	0.15	100
Best	26-Oct-24	1420.89	70.48	400	600.36	100	0	7.41
Best	30-Nov-24	1482.92	73.56	378.57	602.72	96.43	0.08	61.33
Best	07-Dec-24	1533.81	76.08	390.99	604.27	98.51	0.04	40.42
Worst	20-Jul-24	2053.24	101.85	376.09	588.95	97.92	0.06	87.56
Worst	17-Aug-24	2069.53	102.66	381.63	604.17	96.13	0.11	59.55
Worst	14-Sep-24	2107.63	104.55	355.59	599.63	91.07	0.31	100
Worst	06-Jul-24	2244.48	111.33	270.73	600	83.93	0.4	100
Worst	**24-Aug-24**	**2320.18**	**115.09**	**344.42**	**589.6**	**91.37**	**0.38**	**100**
Median	28-Sep-24	1680.42	83.35	355.27	598.34	91.07	0.26	98.81

Specifically, the optimized PI + anti-windup controller satisfied all FCR PQTs and Assessment II criteria, confirming high-fidelity frequency response.

In detail, the WE achieved 100% in-band tracking during normal operation, reached its 400 MW bid within 6.7 s, and sustained at least 90% output for 300 s. Moreover, the robustness analysis verified wide stability margins, ±20 dB gain and ±80° phase. A further support by sensitivity peaks M_s = 1.03 and M_t = 1.01, ensures strong resilience to controller and plant uncertainties.

In later stage, the subsequent long-term scheduling optimization demonstrated that FCR participation reduces the operational hydrogen cost from 103.54 to 86.59 JPY/Nm³, while the best-performing week reached a minimum of 63.77 JPY/Nm³ due to favorable price conditions and high reserve revenues. Furthermore, the daily net expenditure averaged 249 MJPY/ day, with penalties contributing almost 0% of gross FCR revenue. Physically, the hydrogen output remained constant at 529.92 MNm³, and tank utilization demonstrated effective energy-to-hydrogen time-shifting. Furthermore, the thermal performance remained safe, with an average stack temperature of 74.9 °C and 1.38 MW of cooling power.

Although the proposed framework successfully achieves substantial cost reductions and demonstrates regulatory readiness, the obtained hydrogen costs remain significantly above Japan's national targets of 30 JPY/Nm³ by 2030 and 20 JPY/Nm³ by 2050, emphasizing the need for continued innovation. Accordingly, future work may extend this framework to incorporate uncertainty-aware forecasting, hybrid energy storage integration, and policy-based incentive modeling. This aims to close the economic gap and enable large-scale, market-synchronized green hydrogen production.

Acknowledgements

The authors would like to thank the Japan Gas Association for its support of the research.

References

1) Yokoyama, Akihiko. "Toward deregulated, smart and resilient power systems with massive integration of renewable energy in Japan." IEEJ Transactions on Electrical and Electronic Engineering 17.9 (2022): 1242-1254.
2) Asano, Hiroshi, Hideo Ishii, and Hirotaka Takano. "Distributed Energy Resource Integration for Carbon Neutral Power Systems: Market‐Based Approaches to Ancillary Services and Microgrid Operation." IEEJ Transactions on Electrical and Electronic Engineering 19.5 (2024): 598-607.
3) Electrical Power Reserve eXchange (EPRX); https://www.eprx.or.jp/outline/outline.html (Accessed on November 7, 2025)
4) Dozein, Mehdi Ghazavi, Ahvand Jalali, and Pierluigi Mancarella. "Fast frequency response from utility-scale hydrogen electrolyzers." IEEE Transactions on Sustainable Energy 12.3 (2021): 1707-1717.
5) Dozein, Mehdi Ghazavi, Antonella Maria De Corato, and Pierluigi Mancarella. "Virtual inertia response and frequency control ancillary services from hydrogen electrolyzers." IEEE Transactions on Power Systems 38.3 (2022): 2447-2459.

6) Huang, Chunjun, et al. "A review of alkaline electrolyzer technology modeling and applications for decision-making optimization in energy systems." Renewable and Sustainable Energy Reviews 224 (2025): 116005.
7) Huang, Chunjun, et al. "Analytical modeling and control of grid-scale alkaline electrolyzer plant for frequency support in wind-dominated electricity-hydrogen systems." IEEE Transactions on Sustainable Energy 14.1 (2022): 217-232.
8) 中村勇太, et al. "需給調整市場に参入する水電解装置を有するマイクログリッドの運用に関する検討—実績の三次調整力取引価格の時系列データに基づくコスト評価—." エネルギー・資源学会論文誌 43.4 (2022): 172-177.
9) Kaneko, Nanae, et al. "Determining Reserve Power Shared by Each Consumer to Aggregate Solid Oxide Fuel Cells and Storage Batteries for Frequency Containment Reserve." IEEJ Transactions on Electrical and Electronic Engineering 20.8 (2025): 1298-1303.
10) 需給調整市場に係る取引規程等の公表; https://www.eprx.or.jp/outline/docs/guide_250401.pdf (Accessed on November 7, 2025)
11) Van Phan, Long, et al. "Advanced frequency control schemes and technical analysis for large-scale PEM and Alkaline electrolyzer plants in renewable-based power systems." International Journal of Hydrogen Energy 89 (2024): 1354-1367.
12) Phan-Van, L., V. Nguyen Dinh, and T. Nguyen-Duc. "Universal modelling and analysis of grid-scale electrolysers frequency response in wind-dominated power systems." IET Conference Proceedings CP857. Vol. 2023. No. 29. Stevenage, UK: The Institution of Engineering and Technology, 2023.
13) Sharma, Anukriti, and Navdeep Singh. "A cyber-attack resilient load frequency control for two area power system using particle swarm optimized 3-degree-of-freedom–PID controller." Transactions of the Institute of Measurement and Control (2025): 01423312241309066.
14) Qu, Zhengwei, et al. "A multi-source power system's load frequency control utilizing particle swarm optimization." Energies 17.2 (2024): 517.
15) Sakkas, Nikolaos P., et al. "Advanced pressurized alkaline water electrolysis at high temperatures up to 130° C." International Journal of Hydrogen Energy 149 (2025): 150075.
16) Tofighi-Milani, Mahyar, Sajjad Fattaheian-Dehkordi, and Matti Lehtonen. "Electrolysers: A review on trends, electrical modeling, and their dynamic responses." IEEE Access (2025).
17) Graber, Giuseppe, et al. "Day-ahead optimization of proton exchange membrane electrolyzer operations considering system efficiency and green hydrogen production constraints imposed by the European Regulatory Framework." Energies 17.22 (2024): 5713.
18) Electrical Power Reserve eXchange (EPRX); https://www.eprx.or.jp/information/results.php (Accessed on November 7, 2025)
19) Japan Electrical Power eXchange (JPEX); https://www.jepx.jp/en/electricpower/market-data/spot/ (Accessed on November 7, 2025)
20) Seiler, Peter, Andrew Packard, and Pascal Gahinet. "An introduction to disk margins [lecture notes]." IEEE Control Systems Magazine 40.5 (2020): 78-95.